Available online at www.sciencedirect.com
SCIENCE DIRECT®
Biochimica et Biophysica Acta 1612 (2003) 41–51
BIOCHIMICA ET BIOPHYSICA ACTA
BBA
www.bba-direct.com

Effects of alterations of the amino-terminal glycine of influenza hemagglutinin fusion peptide on its structure, organization and membrane interactions

Cheng-Wei Wu[a,1], Shu-Fang Cheng[a,1], Wei-Ning Huang[b], Vishwa Deo Trivedi[a,2], Balakrishnan Veeramuthu[a], Assen B. Kantchev[a], Wen-Guey Wu[b], Ding-Kwo Chang[a,*]

[a] *Institute of Chemistry, Academia Sinica, Taipei 115, Taiwan, ROC*
[b] *Department of Life Sciences, National Tsing Hua University, Hsinchu 30043, Taiwan, ROC*

Received 23 September 2002; received in revised form 27 January 2003; accepted 26 February 2003

Abstract

Mutations of the glycine residue at the amino terminus of HA2 have been shown to have a large effect on the fusion activity of HA2, the extent of which apparently correlates with the side chain bulkiness of the substituting amino acids. To investigate into the cause of abrogation in fusogenicity and virus-promoted fusion mechanism, we synthesized several peptides in which this glycine was substituted by serine, glutamic acid, or lysine. 1,2-Dimyristoyl-*sn*-glycero-3-phosphocholine (DMPC) and 1,2-dimyristoyl *sn*-glycero-3-phosphoglycerol (DMPG) were used as model membranes in the fluorescence, circular dichroism (CD), and FTIR measurements while sodium dodecyl sulfate was used in NMR studies. We found that, for the less active variants, affinity to membrane, degree of solvent dehydration, lipid perturbation, depth of insertion, and helicity were less. Comparison of affinity to membrane bilayer among these analogs revealed that binding of the fusion peptide is determined largely by the hydrophobic effect. Additionally, the orientation is closer to the membrane normal for the wild-type fusion peptide in the helix form while the inactive analogs inserted more parallel to the membrane surface.

Keywords: Membrane fusion; Insertion angle; Insertion depth; Fluorescence quenching; Amide proton exchange

1. Introduction

The hemagglutinin of influenza virus comprises two disulfide-linked subunits, HA1 and HA2, which are responsible for binding to receptor and entry into its target cell, respectively. Viral entry requires fusion between membranes of the virus and the cell in the low pH milieu of endosome [1]. The amino-terminal stretch consisting of ~ 20 amino acid residues, termed fusion peptide, has been implicated in the fusion reaction [2,3]. To delineate the role of this highly conserved sequence in the fusion process, numerous mutations have been made at various positions within the fusion peptide region. The unusually high content of glycine residues and their distribution in the fusion peptide sequence are, in particular, the focus of extensive studies, which included mutations at positions 1, 4, 8, and 13. Among these glycyl residues, glycine 1 and 8 are found more sensitive than the other two in fusogenicity to the mutation [4,5]. The results led to the conclusion that maintaining appropriate helicity is essential for fusion activity of fusion peptides [5]. It was noted that significant helix population, in addition to the β-structure, is necessary for the fusogenic activity of the synthetic fusion peptides [6,7]. A recent study on the Gly 1 variants of HA2 fusion peptide revealed a correlation between the ability of the fusion peptide to lower the bilayer-to-hexagonal phase transition temperature and its ability to promote membrane fusion [8].

It is noteworthy in the work by Gray et al. [6] on the effects of HA2 fusion peptide mutations that insertion at either N- or C-terminal side, as well as substitution with glutamic acid, of the N-terminal glycine resulted in lower helicity and fusogenicity. It demonstrated the extraordinary

* Corresponding author. Tel.: +886-2-2789-8594; fax: +886-2-2783-1237.
E-mail address: dkc@chem.sinica.edu.tw. (D.-K. Chang).
[1] C.W.W. and S.F.C. contribute approximately equivalently to the work.
[2] Present address: Department of Microbiology and Molecular Genetics, University of Texas Medical School, Houston, TX 77030-1501, USA.

0005-2736/03/$ - see front matter © 2003 Elsevier Science B.V. All rights reserved.
doi:10.1016/S0005-2736(03)00084-1

sensitivity of the secondary structure and functions of the fusion peptide to the glycine at position 1. Recently, the effect of substituting Gly 1 with an array of amino acids on the structure and function of HA protein has been examined [9]. With no effect on the cleavage into HA1 and HA2 and on the acid-induced structural change, it was concluded that both the size and hydrophobicity of the side chain were the determinants of the fusion activity. In particular Ser 1 HA, which mediates hemifusion between the viral and target membranes, displays an intermediate phenotype. The importance of Gly 1 was also highlighted by the reversion of Leu 1 HA mutant to Gly or Phe in a reverse genetics study [10]. Substitution of Gly at the N terminus with Val has been found to have a dramatic effect on the orientation of a 20-mer fusion peptide immersed in the membrane bilayer [8]. To understand the underlying structural basis and the membrane interaction mode for the effect of mutation of the amino-terminal residue of HA2 in hope of shedding light on the HA-induced fusion mechanism, we undertook biophysical studies on fusion peptides of Gly 1 variants. We found that, at pH 5.0, binding to liposomes and protection from proteolysis are better while helicity, bilayer lipid perturbation, penetration depth, and angle are different between the wild-type peptide and the inactive homologues. The Ser 1 analog exhibits properties that are intermediate between these two extreme phenotypes. Moreover, both Glu 1 and Lys 1 analogs bind less strongly to the membrane bilayers with different charged headgroup than the wild-type peptide, indicating that binding is dominated by the hydropbobic interaction. These results are further discussed in the context of virus-mediated membrane fusion.

2. Materials and methods

2.1. Materials

The peptides corresponding to residues 1–25 of HA2, G1-HA2(1–25), NH_2-GLFGAIAGFIENGWEGMIDG-WYGFR-COOH (strain X31) of influenza virus and its S1-, E1-, and K1-analogs were synthesized in an automated mode by a solid phase synthesizer from Protein Technologies (Woburn, MA, USA) using 9-fluorenylmethoxycarbonyl (F-moc) chemistry. Cleavage and purification of the peptide were as described previously [7]. 1,2-Dimyristoyl-*sn*-glycero-3-phosphocholine (DMPC) and 1,2-dimyristoyl *sn*-glycero-3-phosphoglycerol (DMPG) were obtained from Avanti Polar Lipids (Alabaster, AL). SDS and d^{25}-SDS were acquired from Boehringer Mannheim (Mannheim, Germany) and Cambridge Isotope (Andover, MA, USA), respectively. Acrylamide, 7-nitrobenz-2-oxa-1,3-diazole (NBD), and proteinase K were purchased from Sigma (St. Louis, MO). 5(6)-Carboxytetramethylrhodamine (rhodamine) was a product from Molecular Probes (Junction City, OR). All reagents were used in the experiments without further purification. Solutions containing vesicles were prepared by solubilizing the lipids in chloroform/methanol (4:1, v/v) mixture and drying the sample under nitrogen stream before dissolving in the buffer solution. Peptide/SDS and peptide/phospholipid mixtures were sonicated for 30–60 min before measurements.

Labeling of the N-terminal residue of the peptide with NBD or rhodamine was performed according to the standard procedure [11], as described in a recent study [7].

2.2. Human erythrocyte lysis experiments

About 10^9 human red blood cells (hRBC) suspended in 10 ml of 100 mM sodium acetate/150 mM NaCl buffer was kept at room temperature in dark. A 200- to 250-μl aliquot of the hRBC stock solution was suspended in 500 μl of the sodium acetate/NaCl buffer followed by addition of each of the 25-mer fusion peptide analogs to make a final peptide concentration of 15 μM. The pH was kept at 4.5 because it has been pointed that the cell fusion activity of the influenza virus was enhanced several fold at pH 4.5 compared to pH 5.2 [11]. The percentage of hemolysis is defined by

$$\% \text{ Hemolysis} = (A_t - A_0)/(A_\infty - A_0) \quad (1)$$

where A_t and A_0 are the absorbances of released hemoglobin at 541 nm at time t and 0 (before adding the peptide), respectively; the maximum absorbance A_∞ is taken from the absorbance obtained with the addition of 10 μl of 0.1% Triton X-100.

2.3. Circular dichroism (CD) experiments

CD experiments for the fusion peptide analogs were carried out on a Jasco 720 spectropolarimeter at room temperature. Spectra were recorded from 184 to 260 nm at a scanning rate of 20 nm min^{-1} with a time constant of 4 s, step resolution of 0.1 nm, and bandwidth of 1 nm. Each of the PBS-buffered peptides was incubated in DMPC:DMPG dispersion (pH 5.0) and sonicated for 30 min before measurements. The final concentration was 10:800:800 μM for HA2:DMPC:DMPG. Cells with path length of 1.0 mm were employed and peptide concentrations were determined with molar absorptivity of 12,660 M^{-1} cm^{-1} at 280 nm [12]. For each of the peptide preparations, the final CD profile was obtained by averaging five scans.

2.4. Attenuated total reflectance (ATR)-FTIR measurements

Each of the tested peptides (20 μg) and DMPC:DMPG (1:1 molar ratio) were mixed in chloroform/methanol (1:1, v/v) solution and equilibrated in PBS buffer at pH 5.0. The final peptide-to-lipid molar ratio was 1:50. The sample was carefully spread on the germanium surface until the solvent had evaporated. The ATR sample covered with a home-made box was kept in full D_2O hydration (D_2O/lipid

ratio>35) based on infrared absorbance ratio of D-O/C-H stretch peaks.

ATR-FTIR spectra were recorded on a Boman DA8.3 spectrometer equipped with a KBr beamsplitter and a liquid nitrogen-cooled MCT detector. The incoming radiation was polarized with a germanium single diamond polarizer (Harrick, Ossining, NY). The 45° germanium ATR-plate (2 mm × 5 mm × 50 mm) was cleaned by plasma cleaner (Harrick, Ossining, NY) before depositing sample. After 300 scans at a spectral resolution of 2 cm^{-1}, the data were treated with triangular apodization.

ATR interface electric field amplitudes are given by [13]:

$$E_x = \frac{2\cos\gamma\sqrt{\sin^2\gamma - n_{21}^2}}{\sqrt{1-n_{21}^2}\sqrt{(1+n_{21}^2)\sin^2\gamma - n_{21}^2}} \quad (2)$$

$$E_y = \frac{2\cos\gamma}{\sqrt{2-n_{21}^2}} \quad (3)$$

$$E_z = \frac{2\cos\gamma\sin\gamma}{\sqrt{1-n_{21}^2}\sqrt{(1+n_{21}^2)\sin^2\gamma - n_{21}^2}} \quad (4)$$

where E_x, E_y, and E_z represent the electric field amplitudes along the x, y, and z axes. n_1 and n_2 are the refractive indices of germanium and a thick film on germanium surface, respectively; $n_{21}=n_2/n_1$; and γ is the angle of incidence between the beam and a normal to the crystal surface, where $n_1=4$, $n_2=1.43$, and $\gamma=45°$.

The infrared linear dichroic ratio is defined by

$$R_z = A_{//}/A_{\perp} = \frac{\langle M_x^2\rangle E_x^2 + \langle M_z^2\rangle E_z^2}{\langle M_y^2\rangle E_y^2} \quad (5)$$

where $A_{//}$ and $A_{\perp}$ are the absorbance for polarized parallel and perpendicular radiation, respectively. M_x, M_y, and M_z are the transition dipole moments along the x, y, and z axes, and a bracket denotes a time and space average over all transition dipole moment during the characteristic time of the IR experiment. Order parameter, S, that describes the orientation distribution of the lipid hydrocarbon chains, S_L, and of the amide I, $S_{\text{amide I}}$, are given by [14]:

$$S_L = -2\frac{E_x^2 - R^{ATR}E_y^2 + E_z^2}{E_x^2 - R^{ATR}E_y^2 - 2E_z^2} \quad (6)$$

$$S_{\text{amide I}} = \left(\frac{2}{3\cos^2\alpha - 1}\right)\left(\frac{E_x^2 - R^{ATR}E_y^2 + E_z^2}{E_x^2 - R^{ATR}E_y^2 - 2E_z^2}\right) \quad (7)$$

where $\alpha=38°$ is taken to be the angle between helix axis and its transition moment [15].

θ, the angle between the molecular axis direction and the ATR crystal normal, is related to S by:

$$S = \left(\frac{3<\cos^2\theta> - 1}{2}\right) \quad (8)$$

2.5. Fluorescence experiments

All fluorescence measurements were performed on a Jasco spectrofluorometer, model FP-777, using a cell of 1 cm in length at 37 °C.

The fluorescence quenching experiments monitored accessibility of the tryptophan residue of the membrane-bound fusion peptide to the acrylamide quencher. An incremental aliquot of acrylamide stock solution (1 M) was added to the peptide solution to make a stepwise increase in the quencher concentration up to 50 mM. The solutions used in these experiments contained 10 μM of the peptide analog, 50 mM NaCl as well as 2.5–4.0 mM SDS or 1.2 mM phospholipid in PBS at pH 5.0. Fluorescence emission spectra in the 300–450 nm range were recorded using 280 nm excitation wavelength with a scan rate of 100 nm min^{-1}, response time of 1 s, and data interval of 0.1 or 0.2 nm. The bandwidths for excitation and emission were 5 and 1.5 nm, respectively. Appropriate blanks were subtracted from the acquired spectra and corrections for dilution were made to the observed fluorescence intensities. The data were analyzed by the Stern–Volmer equation [16]:

$$F_0/F = 1 + K_{SV}[Q] \quad (9)$$

where F_0 is the fluorescence intensity at the zero quencher concentration, F is the fluorescence intensity at any given quencher concentration [Q], and the apparent Stern–Volmer

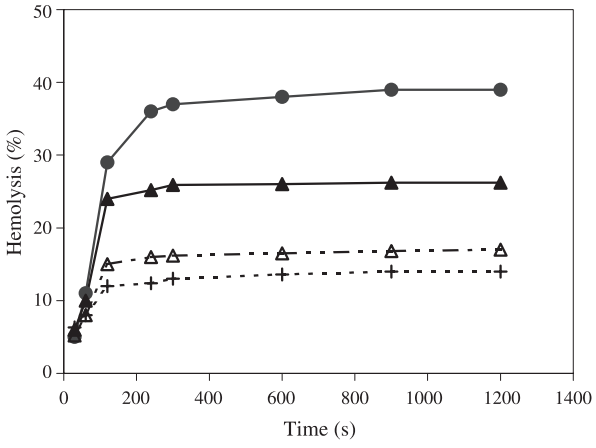

Fig. 1. Hemolytic action of hRBC by G1(●)-; S1(▲)-; E1(△)-; and K1(+)-HA2(1–25) in 100 mM sodium acetate/150 mM NaCl buffer at pH 4.5 at room temperature. The absorption at 541 nm of hemoglobin released from hRBC due to the addition of each of the four fusion peptide analogs was monitored. The maximum absorption value is taken from the value obtained with the addition of 0.1% Triton X-100 to the vesicular dispersion. S1-variant displays an intermediate phenotype among the four analogs tested.

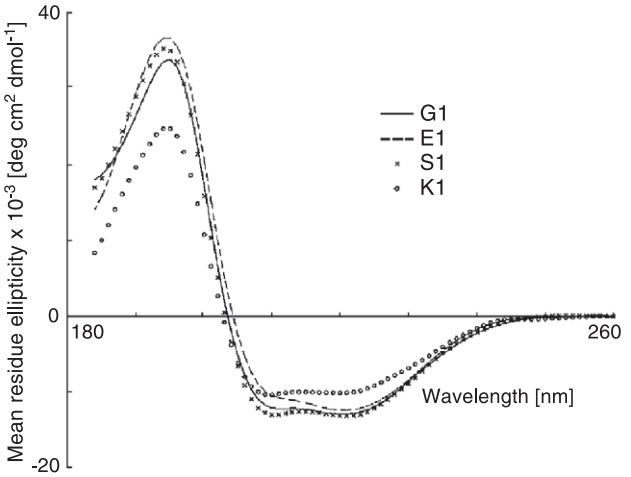

Fig. 2. Far UV-CD spectra of G1-, S1-, E1- and K1-HA2(1–25) in DMPC:DMPG (1:1) at pH 5.0 and room temperature. The peptide-to-lipid molar ratio was 1:160. Slightly higher helical content, represented by the minimum at 222 nm, is found for the G1-analog than E1- and K1-analogs.

quenching constant, K_{SV}, was obtained from the slope of F_0/F vs. [Q] plot. The reported K_{SV} values were the average of two independent measurements.

NBD fluorescence measurements to probe the peptide binding to DMPC and DMPG vesicles were carried out in a suspension containing 1 and 500 μM of the NBD-labeled peptide and phospholipid, respectively at 37 °C. The excitation and emission wavelengths were set at 467 and 528 nm, respectively. The digestive enzyme proteinase K (60 μg/ml) was added to the labeled peptide and vesicle mixture to investigate the extent of protection by the membrane on each of the studied peptides from digestion.

The rhodamine self-quenching experiments were carried out to examine the tendency of self-association of the peptides in PBS and in the vesicular suspension. Briefly, the rhodamine-labeled peptide (2.5 μM) in aqueous buffer at pH 5.0 was mixed with DMPC:DMPG (80:20 μM) vesicles. To monitor the rhodamine probe, the excitation and emission wavelengths were set at 530 and 578 nm, respectively. Digestion of the labeled peptides by proteinase K (6 μM) resulted in an increase in the rhodamine fluorescence intensity due to the disassembly of the membrane-associated oligomeric fusion peptides. The 100% reference intensity was taken from the fluorescence measured in the peptide/lipid dispersion solubilized with 0.2% (v/v) Triton X-100.

2.6. NMR experiments

Micellar suspension containing d^{25}-SDS and each of the 25-mer fusion peptide analogs (100:1.0 mM) were used for one-dimensional and two-dimensional ^{1}H NOESY and TOCSY NMR experiments performed on a Bruker AMX-500 spectrometer, as described previously [17]. In deuteron–hydrogen (D/H) exchange experiments, the peptide-incorporated SDS sample was lyophilized three times with pure H_2O. D_2O:H_2O 9:1 (v/v) was added immediately before acquiring NMR data. Fraction of attenuated back-

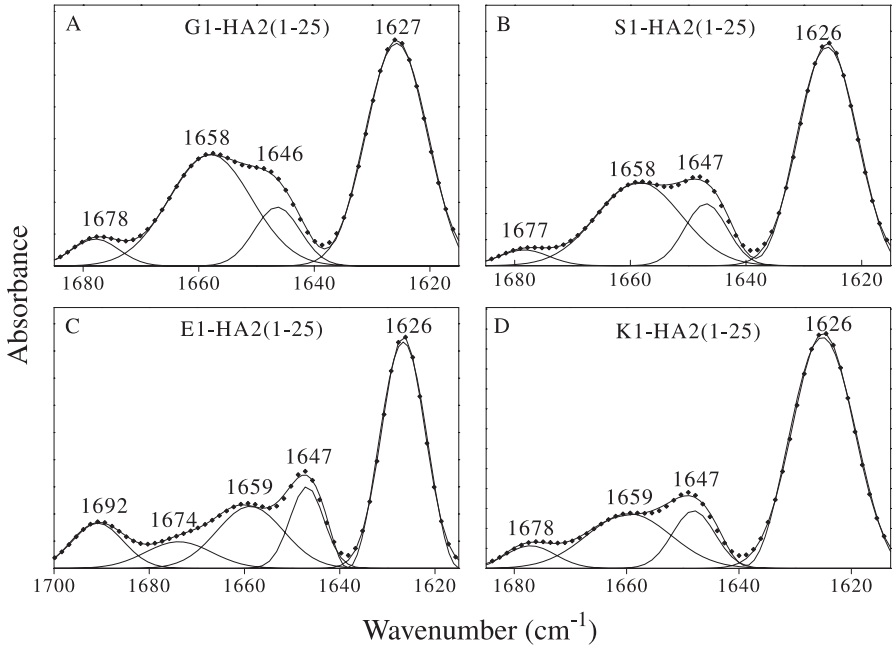

Fig. 3. ATR-FTIR amide I′ contours of the four fusion peptide analogs of influenza virus HA2 embedded in DMPC:DMPG (1:1) planar multilamellar membrane. The peptide-to-lipid molar ratio was 1:50. The optimal parameters used in the Fourier self-deconvolution are 16 for the undeconvoluted band half-width and 2.0 for resolution enhancement factor. The individual curve-fitting Gaussian bands and their sum are represented as solid and dotted lines, respectively. Helical population is higher for G1- and S1-HA2(1–25) than for E1- and K1-peptides. This result suggests that a significant helix content or ratio of α to β conformation is necessary for the fusion activity of the influenza fusion peptide.

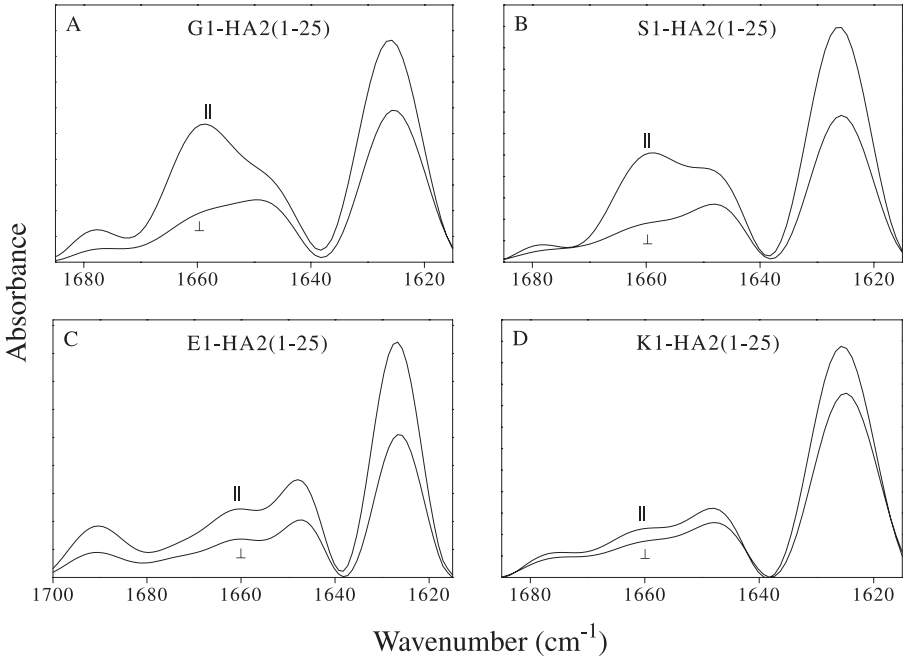

Fig. 4. Polarized ATR-FTIR spectra of G1-, S1-, E1-, and K1-HA2(1–25) in DMPC:DMPG (1:1) planar multilamellar membrane at pH 5.0. A large difference between the parallel (∥) and perpendicular (⊥) polarized absorbances at 1658 cm^{-1} band is observed for the fusion active G1- and S1-analogs. In marked contrast, the difference is much smaller for the inactive E1- and K1-mutants. Thus, the order parameters derived from the dichroic ratios are positive for G1- and S1-analogs as opposed to the negative values for E1- and K1-analogs. This indicates that there is a substantial difference in the angle formed by the helix axis and membrane normal for the former two peptides as compared to the latter two.

bone amide proton is taken as the fractional difference in the crosspeaks of NH/αH or side chain protons of a given residue obtained for the protonated and deuterium-exchanged d^{25}-SDS micellar solution.

3. Results

3.1. Hemolytic effects of the HA2 fusion peptide analogs

Influenza virus has been shown to markedly enhance hemolysis at low pH [18]. To see if the property is retained for the fusion peptides, we carried out hemolytic measurements using hRBC suspension incubated with each of the peptide analogs. Fig. 1 shows that the hemolytic activity is the lowest for E1- and K1-HA2(1–25) and highest for the wild-type G1-HA2(1–25) with S1-analog between these two classes. The result is in line with the trend in the fusion activity found for the fusion proteins to which these peptides correspond [9]. In particular, the S1-variant of HA2 exhibited an intermediate phenotype on fusion of HA-containing cells and target membranes [10].

3.2. Secondary structure determination of the peptide analogs in lipid bilayer by CD and ATR-FTIR spectroscopy revealed higher helicity for the wild-type peptide

CD experiments on G1-, S1-, E1- and K1-HA2(1–25) peptides indicate higher helix content for the wild-type peptide in DMPC:DMPG dispersion. Fig. 2 illustrates far UV-CD spectra of the four 25-mer peptides in 1:80:80 (molar ratio) peptide:DMPC:DMPG vesicular solution at room temperature, pH 5.0. Analysis of the spectra using Hennessey and Johnson secondary structure prediction algorithm [12] yielded helix content of 38% for G1- and S1-HA2(1–25) and 30% for the E1- and K1-variants, qualitatively in agreement with previous studies on slightly shorter HA2 fusion peptides showing a slightly higher helicity for the fusion active wild-type analog [6,19,20].

To further investigate the secondary structure elements of the 25-mer peptides, ATR-FTIR measurements were conducted on the peptides embedded in the multilamellar

Table 1
Secondary structure and helix axis orientation derived from ATR-FTIR spectra of G1-, S1-, E1-, and K1-HA(1–25) in DMPC:DMPG (1:1) multilamellar bilayers at pH 5.0[a]

	G1	S1	E1	K1
Secondary percentage				
α-Helix	33 ± 1	30 ± 1	20 ± 3	20 ± 1
Disorder	11 ± 3	11 ± 3	15 ± 1	11 ± 1
β-Sheet	50 ± 1	54 ± 1	59 ± 3	63 ± 1
β-Turn	6 ± 1	4 ± 1	6 ± 7	6 ± 1
Helix axis orientation				
R^{ATR}	2.6 ± 0.6	2.8 ± 0.1	1.6 ± 0.1	1.5 ± 0.1
$S_{amide\ I'}$	0.36 ± 0.04	0.43 ± 0.06	− 0.31 ± 0.1	− 0.43 ± 0.1
Θ	41°	38°	70°	78°

[a] The peptide-to-lipid molar ratio was 1:50.

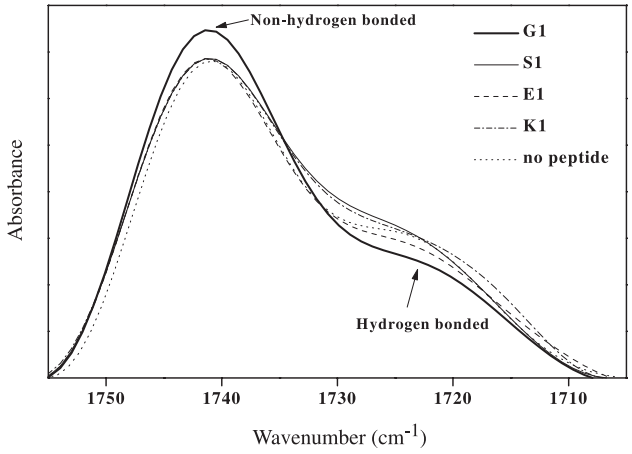

Fig. 5. Lipid ester carbonyl stretching region of the ATR-FTIR spectra of DMPC/DMPG (1:1) multilayers alone and multilayers containing each of G1-, S1-, E1-, and K1-HA2(1–25). Measurements were made at pH 5.0 and lipid-to-peptide ratio is 50:1. After the Fourier-self deconvolution, the region is decomposed into two component bands at around 1742 and 1726 cm^{-1}, which are assigned to the non-hydrogen bonded and hydrogen bonded carbonyl stretching vibrations, respectively. Higher free carbonyl component is seen for G1-analog in association with the membrane, implying higher degree of membrane surface dehydration.

membrane. Fig. 3 shows the spectra in the amide I′ band region which is sensitive to the secondary structure of the peptides. All four analogs exhibit distinct bands centered at 1627, 1645, 1658, and 1676 cm^{-1} after treatment of the data by Fourier self-deconvolution and Gaussian curve-fitting [21]. They are assigned to β-sheet, random coil, α-helix, and β-turn, respectively [22–24]. For the E1-analog, an additional minor band at 1692 cm^{-1} can be discerned which may be attributed to β-structure [25]. In agreement with the CD result, a higher helix (1658 cm^{-1}) content is found for G1- and S1-analogs that are more fusion active. On the other hand, the data reveal higher β-sheet content for the inactive E1- and K1-analogs with a dominant band at 1627 cm^{-1}.

3.3. G1- and S1-HA2(1–25) helices bound to membrane bilayer is aligned closer to the membrane normal than the other two analogs

Polarized ATR-FTIR measurements were used to determine the orientation of the helix structure that penetrates into the membrane bilayer. Fig. 4 illustrates infrared absorption spectra of the parallel and perpendicular polarized lights for the four peptides in the DMPC:DMPG (1:1) planar multilamellar membrane at pH 5.0, and the results are analyzed and summarized in Table 1. The order parameters for G1- and S1-analogs are 0.36 and 0.43, respectively, while those for E1- and K1-analogs are −0.31 and −0.43, respectively. The angles formed between the helix axis and the membrane normal are calculated to be 41° and 38°, respectively, for the former two peptides, while those for the other two are 70° and 78°, respectively. It is of interest to note that the active fusion peptide analogs insert obliquely into the phospholipid bilayer, whereas the inactive peptides adopt an angle more parallel to the bilayer surface. The data thus imply a shallower insertion into the membrane for the inactive peptides than for the active ones.

3.4. Influence of the four membrane-bound analogs on the acyl chain order and ester carbonyl groups of the phospholipid bilayer

We further investigated the effect of these membrane-bound peptides on the ester carbonyl groups and on the order of hydrocarbon chains of the lipid bilayer by examining the regions at 1755–1705 and 3050–2800 cm^{-1}, respectively. The bands at 1742 and 1726 cm^{-1} are thought to arise from free carbonyl group and hydrogen-bonded carbonyl group, respectively [6,26]. Fig. 5 displays the resolved ester carbonyl bands in the presence, and in the absence, of each of the peptides tested. The free component is larger in the presence of G1-HA2(1–25) than other peptides or in the absence of bound peptides. Assuming that 1726 cm^{-1} band is due to the carbonyl moiety hydrogen-bonded to the water molecule, this observation suggests a higher degree of bilayer dehydration induced by the associated wild-type peptide (see Discussion). Results on the analyzed polarized vibrational spectra of the methylene groups on the lipid hydrocarbon chain are summarized in Table 2. Comparison of the order parameters derived from the lipid methylene antisymmetric stretching vibration band (~ 2921 cm^{-1}) in the presence of each of the peptides tested and in their absence reveals that all the peptide analogs cause an increase in the order parameters with the G1-analog

Table 2
Polarized ATR-FTIR dichroic ratios and order parameters calculated from the antisymmetric vibration bands of methylene groups of DMPC:DMPG multilamellar bilayers in the presence of each of the HA2 fusion peptide analogs and in its absence[a,b]

$\nu_{antisymmetric}$ (CH_2)	G1	S1	E1	K1	–[c]
R^{ATR}	0.97 ± 0.04	1.13 ± 0.01	1.08 ± 0.02	1.16 ± 0.10	1.20 ± 0.01
S_L	0.86 ± 0.04	0.68 ± 0.01	0.73 ± 0.02	0.65 ± 0.10	0.61 ± 0.01

[a] The experiments were performed in the DMPC:DMPG (1:1) vesicular solution with lipid-to-peptide ratio of 50:1 at pH 5.0 and room temperature.
[b] The larger change in dichroic ratio and increase in the order of acyl chain of the lipid represents greater perturbation of the G1-analog to the membrane bilayer than the other peptide variants.
[c] No peptide was added.

showing the largest effect. The result corroborates a study on the role of the hydrophobic residues in the central region of HA2 fusion peptide sequence in that the fusogenic analogs caused an increased acyl chain order [5].

3.5. Measurements of tryptophan fluorescence quenching indicate penetration of the peptides into the lipid bilayer

Tryptophan fluorescence quenching by acrylamide was used to probe the insertion depth of the 25-mer fusion peptide analogs. Note that in Table 3, for the peptides tested, K_{SV} values in the PBS solution are considerably larger than those in SDS or vesicular dispersion. Because the degree of aggregation is much higher in the aqueous medium than in the lipid bilayer (Ref. [26a]; cf. also Fig. 7), larger K_{SV} values in PBS solution do not arise from shielding of the quencher from the Trp residues due to peptide aggregation; rather, they stem from embedding of the peptides in the lipid bilayer. No clear trend for the peptides tested is observed for K_{SV} in DMPG dispersion but a smaller K_{SV} is obtained with the G1-analog embedded in DMPC suspension. The latter result suggests a deeper insertion for the wild-type peptide in the DMPC dispersion.

3.6. Membrane binding studies using NBD fluorescence

NBD fluorescence was used to probe binding between peptides and lipid [7,27]. Because the fluorescence of the NBD moiety is sensitive to environment, each of the labeled peptides, when added to vesicles, exhibits an increase in the fluorescence intensity concomitant with a blue shift in the emission wavelength (Fig. 6). It indicates that the N-terminal segments of all NBD-labeled peptides insert into the hydrophobic core of the model membrane. As listed in Table 3, the wild-type peptide has highest affinity to both DMPC and DMPG vesicles and is better protected from the enzyme digestion than the other peptides. Because stronger interaction is found for G1-HA2(1–25) regardless of the charge on the phospholipid headgroup or the polarity of the N-terminal residue of the peptide, it is clear that the hydrophobic effect plays a dominant role in the peptide binding to the vesicle.

Table 3
Fluorescence measurements on the fusion peptide analogs of HA2(1–25) in aqueous buffer, SDS micelles, DMPG, and DMPC vesicular dispersions at pH 5

	Media	G1	S1	E1	K1
Acrylamide quenching of tryptophan fluorescence (K_{SV}, M^{-1})	PBS	15.0	15.0	16.2	16.2
	SDS	10.8	10.8	14.3	12.9
	DMPG	8.7	8.1	7.7	9.0
	DMPC	4.6	6.1	6.2	6.0
NBD binding to DMPC and DMPG dispersions (in %)[a]	DMPC	100	26	21	38
	DMPG	65	33	15	33
Protection of the peptides bound to DMPC and DMPG vesicles from cleavage by proteinase K (in %)[a]	DMPC	69	16	12	24
	DMPG	57	28	15	32

[a] Relative NBD fluorescence. The intensity obtained with G1-analog in DMPC suspension was taken as 100%.

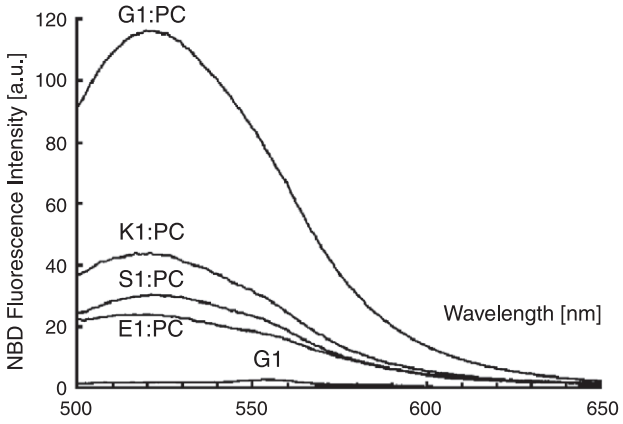

Fig. 6. Fluorescence enhancement of NBD upon mixing NBD-labeled 25-mer fusion peptide analogs of HA2 with lipid bilayers at pH 5.0 and 37 °C. Each of the peptide stock solution was added to DMPC dispersion to make final concentrations of 1 and 500 μM for the peptide and lipid, respectively. The emission profiles for S1-, E1-, and K1-HA2(1–25) solutions in aqueous buffer are virtually the same as that of G1-peptide solution and therefore omitted for clarity. Note the blue shift and dramatic increase in NBD fluorescence for the labeled peptides, particularly the wild-type peptide, in association with the lipid bilayer.

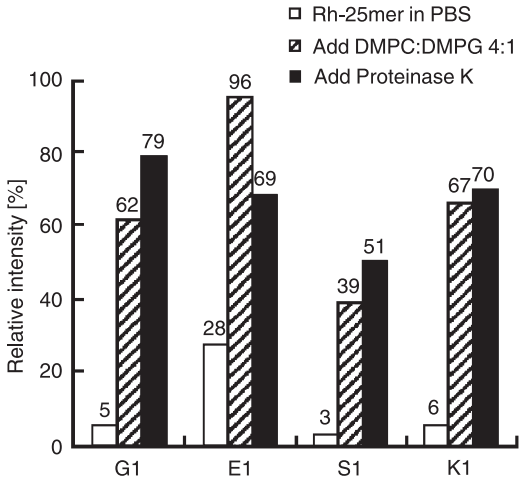

Fig. 7. Self-association of the 25-mer fusion peptide analogs of HA2 in DMPC:DMPG (4:1) vesicles at pH 5.0 and 37 °C as probed by fluorescence self-quenching of rhodamine attached to the N terminus of the peptides. All four vesicle-associated labeled peptides in the membrane-bound state exhibited moderate dequenching when solubilized by Triton X-100 indicating a loose oligomerization for these four peptides tested. Compact packing or aggregation of all the peptides tested is manifested by a highly quenched rhodamine fluorescence in aqueous buffer solution.

3.7. Use of rhodamine fluorescence to probe the oligomerization propensity of the peptide analogs in the lipid bilayer

Self-quenching of rhodamine fluorescence was used to monitor self-assembly of the fusion peptide analogs labeled with the rhodamine probe. As illustrated in Fig. 7, for all the peptides tested, fluorescence is severely quenched in aqueous buffer as a result of high order and tightly packed aggregation [26a]. Solubilization of the labeled peptides by the lipids results in an increase in rhodamine fluorescence intensity. Further moderate rhodamine fluorescence enhancement with the treatment of proteinase K and Triton X-100 is indicative of a loose self-assembly for the peptides in the membranous environment. However, no clear trend in the oligomeric state is found among these four analogs.

3.8. Interaction of the fusion peptides with SDS micelle as monitored by the amide proton exchange rate obtained from NMR spectroscopy

Fig. 8 displays proton resonance intensity attenuation results of the backbone amide protons of residues arising from exchange by deuterium for the four 25-mer peptide analogs in the SDS micellar solution at pH 5.0. The data show that E1- and K1-HA2(1–25) penetrate more shallowly into SDS micelle than G1- and S1-analogs. It is clear that residues 2–10 of G1-peptide are embedded in the interior, whereas E1- and K1-peptides are more solvent accessible for this region because the amide protons from these residues underwent slower exchange for the G1-analog. It is noteworthy that the S1-analog displays intermediate phenotype. The exchange rate for E1- and K1-peptides also exhibits periodicity of an α-helix in the residues 2–10 segment; thus, residues 4, 5, and 8 are on the water-facing side, whereas residues 3, 6, 7, 9, and 10 point toward the hydrophobic core of the micelle. This also corroborates the IR (Table 1) and the tryptophan fluorescence quenching (Table 3) data indicating shallower penetration for the two inactive peptides. We also note that amide protons of Met 17 and Ile 18 exhibited slower exchange compared to those of adjacent residues for all the peptide analogs under investigation here and in our previous study [7] on the binding mode of G1-HA2(1–25) showing that residues 16–18 are located near the micelle/water interface. It is likely that, for E1- and K1-analogs, residues 11–15 are closer to the headgroup region than the wild-type peptide when associating with SDS micelle, consistent with a shallower penetration for the former two peptides as deduced from ATR-FTIR experiments.

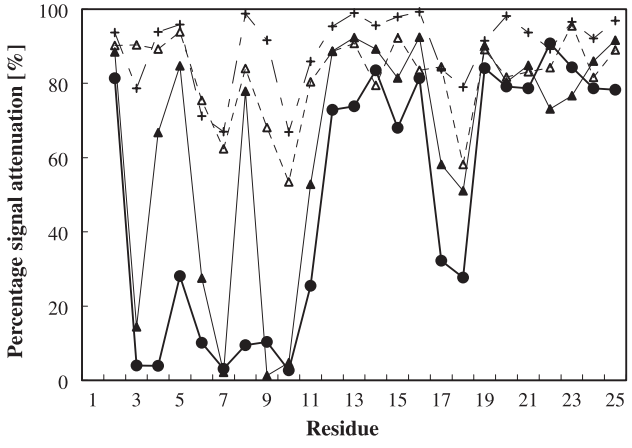

Fig. 8. Backbone amide proton/deuterium exchange measurements as a probe for the interaction mode of influenza 25-mer fusion peptide variants. Note that S1(▲)-; E1(△)-; and K1(+)-HA2(1–25) display α-helical periodicity in the exchange rate within the segment 2–10, in contrast to a more uniform and slower exchange for the wild-type variant, G1(●)-HA2(1–25). The exchange rate in the N-terminal region is faster for E1- and K1-analogs than S1- or G1-analogs. The result suggests shallower penetration into SDS micelle for the former two inactive peptides, possibly as a consequence of insertion of helix with an orientation more parallel to membrane surface. The depth of insertion of S1-HA2(1–25) is between that of G1- and E1- or K1-peptides. Data on G1-HA2(1–25) are adapted from Chang et al., J. Biol. Chem. 275 (25) (2000) 19150, with permission.

4. Discussion

To examine the role of the N-terminal glycine in the fusion activity of HA2 and to gain insight into the mechanism of influenza virus-mediated fusion, we synthesized serine, glutamate, and lysine-substituted N-terminal analogs of the 25-mer fusion peptide of HA2. It was observed that the S1-mutant of the influenza fusion protein exhibited an intermediate phenotype, that is, hemifusion, whereas E1-, K1-, and V1-analogs lost the fusion capability completely [9]. The result indicated that a small size of the substituting amino acid is critical for hemifusion, while many polar and bulky residues abrogate fusogenicity completely. The 25-mer fusion peptide analogs studied here showed varied degree of hemolytic activity (Fig. 1) in the same order as the activity of the corresponding fusion proteins, suggesting that fusion peptide fragments can in some aspect mimic the properties of fusion proteins.

Results of the tryptophan fluorescence quenching with acrylamide (Table 3) for these four HA2 fusion peptide analogs show that insertion into DMPC is deeper than into DMPG for a given peptide and the wild-type peptide penetrates deeper than the rest of the peptides tested. These data are consistent with ATR-FTIR results in that G1-HA2(1–25) inserts obliquely into the lipid bilayer with an angle closer to the membrane normal than the E1- or K1-analog does (Table 1). This observation is in line with the concept that tilted insertion of a fusion peptide helix is a common mode for membrane destabilization and fusion [28–30]. Likewise, NMR H/D exchange measurements yielded that E1- and K1-analogs are more solvent-exposed when bound to SDS micelles. We also observed higher helix content and less β-structure for the two more active 25-mer

peptides from CD and ATR-FTIR measurements, in agreement with a previous study [6] on the secondary structure of G1- and E1-HA2(1–23). Taken together, it appears that deeper insertion into the membrane correlates with higher helicity for the fusion peptides [19], and binding affinity and angle of insertion can influence the fusion activity. This notion is in agreement with previous findings that the helical structure is enhanced upon associating with the membrane for the fusion peptides of influenza and human immunodeficiency viruses [7,17,19], although high helicity alone is not sufficient for fusion activity [5]. The present result supports the proposal that a dynamic equilibrium between helix and non-helix forms of fusion peptide in the membrane environment is essential for the fusion process [6,7,31]. Our data on the angle of insertion in Table 1 also suggest that an orientation of the fusion peptide helix close to ($\sim 40°$) the membrane normal may be important in the hemifusion stage of membrane fusion, because S1-variant displays a 38° angle. A recent biophysical study on a 20-mer HA2 fusion peptide attached to a highly charged seven-residue sequence concluded that the fusion peptide had an inverted 'V'-shaped helix at pH 5 in dodelcylphosphocholine micellar solution deduced from NMR data and immersed in the lipid bilayer with an angle of 53° to the membrane normal from the EPR measurement [32]. Our data on the G1-peptide showed a tilt angle of 41° to the membrane normal, in close agreement with 39° obtained by Gray et al. [6] and 45° by Lüneberg et al. [35] from FTIR measurements on slightly shorter fusion peptide fragments of HA2. The discrepancy could be in part due to the fact that the membrane was planar in different hydration state in FTIR measurements, whereas the EPR experiment was carried out in the large unilamellar vesicle by Han et al. [32].

Comparison of the 2921 cm^{-1} peak in the infrared spectra of phospholipid (the antisymmetric methylene stretching vibration of the lipid hydrocarbon chains) in the presence and absence of the fusion peptide analogs indicates a more significant perturbation on the lipid caused by G1-HA2(1–25) than the other analogs (Table 2). The result is compatible with a report on the relation between the infectivity of influenza virus and its ability to perturb the lipid by Epand and Epand [34] using ^{31}P NMR. On the other hand, the free component of ester carbonyl stretching vibration (1742 cm^{-1}) is larger for the G1-analog-containing lipid (Fig. 5). The 1726 cm^{-1} band can be ascribed to lipid ester carbonyl group hydrogen-bonded either to solvent or to the hydrogen donor on the peptide side chain such as that of asparagines, aspartic acid, or glutamic acid at low pH. It is not likely that G1-HA2(1–25) having highest affinity (Table 3) and perturbation to the lipid bilayer (Table 2) would give rise to a larger free component of ester carbonyl vibration from weaker peptide–lipid interaction. Therefore, we believe that the 1726 cm^{-1} band is primarily solvent-originated. Hence, an increased ratio of the 1742 to 1726 cm^{-1} bands due to the addition of the G1-peptide to lipid bilayer, as demonstrated in Fig. 5, indicates a higher dehydration induced by the presence of G1-HA2(1–25) while other analogs exert less significant effect. By incorporating FTIR data on S1- and K1-analogs in addition to data on G1- and E1-analogs [6], we are able to draw a conclusion that there is a discernible, albeit not dramatic, effect on increasing the lipid chain order for the wild-type peptide while less for the other three variants. The result suggests that a perturbation to membrane hydrocarbon core by the bound fusion peptide is necessary for the influenza hemagglutinin to induce complete membrane fusion. Because dehydration at the membrane surface is known to be associated with an increase in acyl chain order [36], our data in Table 2 are consistent with those shown in Fig. 5 in that the wild-type peptide gives rise to the largest increase in the order parameter and highest degree of dehydration among the peptide variants tested.

Experiments on binding of the peptides to the lipid bilayer as monitored by NBD fluorescence and proteinase K digestion experiments (Table 3) shows, as expected, higher affinity to the bilayer for the more active G1-analog while much lower for S1-, E1-, and K1-analogs. Because among the four N-terminal variants only the wild-type HA2 mediates full fusion, it is tempting to postulate that higher density of membrane-bound fusion peptides may be instrumental in the later stage of the fusion reaction, namely, the transition from hemifusion to full fusion. The rationale is that higher fusion peptide density would facilitate fusion pore formation, an essential step in the content mixing process or complete fusion. The lower helicity of E1- and K1-HA2(1–25) in the vesicular dispersion exhibited in CD and FTIR data (Figs. 2 and 3) is probably due in part to smaller portion of membrane-bound peptide, because membrane-binding is known to induce helix for HA2 fusion peptide [19]. Membrane attachment of a solubilized bromelain-treated HA was found independent of lipid composition and divalent cation by Doms et al. [33], implying a hydrophobic interaction-dominant binding; thus, the fusion peptide may be a major membrane-binding domain for HA because the fusion peptide displays a similar binding property. A minor role of electrostatic interaction in the fusion peptide binding to membrane was supported by an insignificant increase in NBD fluorescence with added salt up to 1 M (S.F.C. and D.K.C., unpublished data).

Our rhodamine fluorescence data in Fig. 7 demonstrating the self-assembly propensity of G1-HA2(1–25) support the idea of the cooperativity of HA trimers during hemagglutinin-mediated membrane fusion. Among the four peptides considered here, however, we did not observe a close correlation between the tendency for self-assembly and fusogenicity.

The backbone amide H/D exchange rate measurements in the SDS micellar suspension (Fig. 8) exhibit a distinction mainly in the segment 2–10 among the four peptide analogs. In analogy to the previous result on G1-peptide [7], all four peptides inserted into the SDS micelle, albeit with different depths. The insertion into the SDS micelle for

this segment is deeper for the wild-type peptide than the S1-analog, based on the observation that S1-analog displays a periodic variation with the helical pitch in the exchange rate (residues 3, 6, 7, 9, and 10 show slower H/D exchange) while G1-analog does not. The acrylamide quenching data on these analogs also point to a deeper immersion of the wild-type peptide in the phospholipid vesicle.

We have inferred from CD and NMR experiments that conformational equilibrium occurs for the inserted domain of HA2, which also self-associates loosely in the membranous setting [7]. We note that the observed CD, NMR, and IR data are quantities averaged over the participating states, with different emphasis for these techniques. For example, the NMR amide H/D exchange results may reflect more the condition in the monomeric than the associated state because the exchange rate is presumably faster in the former state than in the latter.

Regardless of the charge on the side chain, both E1- and K1-variants exhibit a lower helix content, shallower penetration into and weaker binding to the vesicles (Tables 1 and 3) or micelle (Fig. 8), and less membrane dehydration (Table 2 and Fig. 5). These factors may contribute to the abolishment of fusogenicity of the corresponding HA mutants. The opposite charge on E1- and K1-analogs enabled us to conclude that the hydrophobic effect plays a dominant role in fusion peptide–membrane interaction. It is likely that the bulky side chains of Glu and Lys mediate membrane interaction in a manner different from that of Gly (or Ala). In accord with the idea that the size of the side chain of the N-terminal residue of HA2 fusion peptide is more important than polarity in modulating the fusion activity [9], we also found that the side chain size is more critical in modulating the structure of fusion peptide and its interaction with membrane. Further investigation into the altered membrane properties with these analogs would be useful in unraveling HA-mediated fusion. For example, headgroup spacing of the target membrane was an important parameter in determining liposome fusion induced by an 11-mer model peptide coupled to a lipid molecule [37].

Based on our investigation on the variants at the position 1 of the fusion peptide of influenza, we propose that there are at least the following factors important for the peptide-mediated membrane mixing or fusion: depth and angle of insertion, substantial helicity, membrane binding affinity, dehydration of membrane surface, and increased lipid chain order. Additional factors such as the composition of lipid can also influence membrane fusion. For example, lysophosphatidylcholine is known to interfere with the formation of hemifusion diaphragm and inhibit the fusion reaction at an early stage, while oleic acid decreases the energy barrier of hemifusion reaction resulting in an enhanced rate and extent of bilayer fusion [38]. More detailed study on the interaction of fusion protein and the lipid bilayer [39]—for instance, the mechanism whereby tilted fusion peptide promotes membrane fusion—should yield more information on the HA-mediated fusion mechanism.

Acknowledgements

This work was supported by Academia Sinica and National Science Council, (NSC89-2113-M-001-076), Taiwan, Republic of China. We thank the Instrument Center at Hsinchu National Tsing Hua University for the Infrared work.

References

[1] J.M. White, Membrane fusion, Science 258 (1992) 917–924.
[2] T. Weber, G. Paesold, C. Galli, R. Mischler, G. Semenza, J. Brunner, Evidence for H(+)-induced insertion of influenza hemagglutinin HA2 N-terminal-segment into viral membrane, J. Biol. Chem. 269 (1994) 18353–18358.
[3] S.A. Wharton, L.J. Calder, R.W. Ruigrok, J.J. Skehel, D.A. Steinhauer, D.C. Wiley, Electron microscopy of antibody complexes of influenza virus haemagglutinin in the fusion pH conformation, EMBO J. 14 (1995) 240–246.
[4] D.A. Steinhauer, S.A. Wharton, J.J. Skehel, D.C. Wiley, Studies of the membrane fusion activities of fusion peptide mutants of influenza virus hemagglutinin, J. Virol. 69 (1995) 6643–6651.
[5] X. Han, D.A. Steinhauer, S.A. Wharton, L.K. Tamm, Interaction of mutant influenza virus hemagglutinin fusion peptides with lipid bilayer: probing the role of hydrophobic residue size in the central region of the fusion peptide, Biochemistry 38 (1999) 15052–15059.
[6] C. Gray, S.A. Tatulian, S.A. Wharton, L.K. Tamm, Effect of the N-terminal glycine on the secondary structure, orientation, and interaction of the influenza fusion peptide with lipid bilayers, Biophys. J. 70 (1996) 2275–2286.
[7] D.K. Chang, S.F. Cheng, V.D. Trivedi, S.H. Yang, The amino-terminal region of the fusion peptide of influenza virus hemagglutinin HA2 inserts into sodium dodecyl sulfate micelle with residues 16–18 at the aqueous boundary at acidic pH, J. Biol. Chem. 275 (2000) 19150–19158.
[8] R.M. Epand, R.F. Epand, I. Martin, J.M. Ruysschaert, Membrane interaction of mutated forms of the influenza peptide, Biochemistry 40 (2001) 8800–8807.
[9] H. Qiao, R.T. Armstrong, G.B. Melikyan, F.S. Cohen, J.M. White, A specific point mutant at position 1 of the influenza hemagglutinin fusion peptide displays a hemifusion phenotype, Mol. Biol. Cell 10 (1999) 2759–2769.
[10] K.J. Cross, S.A. Wharton, J.J. Skehel, D.C. Wiley, D.A. Steinhauer, Studies on influenza haemagglutinin fusion peptide mutants generated by reverse genetics, EMBO J. 20 (2001) 4432–4442.
[11] D. Rapaport, Y. Shai, Aggregation and organization of pardaxin in phospholipid membranes, J. Biol. Chem. 267 (1992) 6502–6509; J. Ramalho-Santos, S. Nir, N. Duzgunes, A.P. deCarvalho, M.daC. deLima, A common mechanism for influenza virus fusion activity and inactivation, Biochemistry 23 (1993) 2279–2771.
[12] W.C. Johnson, Protein secondary structure and circular dichroism: a practical guide, Proteins 7 (1990) 205–214.
[13] N.J. Harrick, Internal Reflection Spectroscopy, Wiley, New York, 967.
[14] L.K. Tamm, S.A. Tatulian, Orientation of functional and nonfunctional PTS permease signal sequences in lipid bilayers. A polarized attenuated total reflection infrared study, Biochemistry 32 (1993) 7720–7726.
[15] D. Marsh, M. Muller, F.J. Schmitt, Orientation of the infrared transition moments for an α-helix, Biophys. J. 78 (2000) 2499–2510.
[16] J.R. Lakowicz, Principles of Fluorescence Spectroscopy, Plenum, New York, 1983.
[17] D.K. Chang, S.F. Cheng, W.J. Chien, The amino-terminal fusion domain peptide of human immunodeficiency virus type 1 gp41 inserts

into the sodium dodecyl sulfate micelle primarily as a helix with a conserved glycine at the micelle–water interface, J. Virol. 71 (1997) 6593–6602.
[18] T. Maeda, S. Ohnishi, Activation of influenza virus by acidic media causes hemolysis and fusion of erythrocytes, FEBS Lett. 122 (1980) 228–283.
[19] J.D. Lear, W.F. DeGrado, Membrane binding and conformational properties of peptides representing the NH2 terminus of influenza HA-2, J. Biol. Chem. 262 (1987) 6500–6505.
[20] S.A. Wharton, S.R. Martin, R.W. Ruigrok, J.J. Skehel, D.C. Wiley, Membrane fusion by peptide analogues of influenza virus hemagglutinin, J. Gen. Vriol. 69 (1988) 1847–1857.
[21] Y.H. Lin, W.N. Huang, S.C. Lee, W. Wu, Heparin reduces the α-helical content of cobra basic phospholipase A_2 and promotes its complex formation, Int. J. Biol. Macromol. 27 (2000) 171–176.
[22] D.M. Byler, H. Susi, Examination of the secondary structure of proteins by deconvolved FTIR spectra, Biopolymer 25 (1986) 469–487.
[23] M. Jackson, H.H. Mantsch, The use and misuse of FTIR spectroscopy in the determination of protein structure, Crit. Rev. Biochem. Mol. Biol. 30 (1995) 95–120.
[24] L.K. Tamm, S.A. Tatulian, Infrared spectroscopy of proteins and peptides in lipid bilayers, Q. Rev. Biophys. 30 (1997) 365–429.
[25] R. Khurana, A.L. Fink, Do parallel β-helix proteins have a unique Fourier transform infrared spectrum? Biophys. J. 78 (2000) 994–1000.
[26] R.N.A.H. Lewis, R.N. McElhaney, W. Pohle, H.H. Mantsch, Components of the carbonyl stretching band in the infrared spectra of hydrated 1,2-diacylglycerolipid bilayers: a reexamination, Biophys. J. 67 (1994) 2367–2375.
[26a] D.K. Chang, S.F. Cheng, V.D. Trivedi, Conformation and interaction with the membrane models of the amino-terminal peptide of influenza virus hemagglutinin HA2 at fusion pH, Arch. Biochem. Biophys. 396 (2001) 89–98.
[27] O. Samuel, Y. Shai, Participation of two fusion peptides in measles virus-induced membrane fusion: emerging similarity with other paramyxoviruses, Biochemistry 40 (2001) 1340–1349.
[28] M. Horth, B. Lambrecht, M.C. Khim, F. Bex, C. Thiriart, J.M. Ruysschaert, A. Burny, R. Brasseur, Theoretical and functional analysis of the SIV fusion peptide, EMBO J. 10 (1991) 2747–2755.
[29] R. Brasseur, Tilted peptides: a motif for membrane destabilization (hypothesis), Mol. Membr. Biol. 17 (2000) 31–40.
[30] S.A. Tatulian, P. Hinterdorfer, G. Baber, L.K. Tamm, Influenza hemagglutinin assumes a tilted conformation during membrane fusion as determined by attenuated total reflection FTIR spectroscopy, EMBO J. 14 (1995) 5514–5523.
[31] X. Han, L.K. Tamm, pH-dependent self-association of influenza hemagglutinin fusion peptides in lipid bilayers, J. Mol. Biol. 304 (2000) 953–965.
[32] X. Han, J.H. Bushweller, D.S. Cafiso, L.K. Tamm, Membrane structure and fusion-triggering conformation change of the fusion domain from influenza hemagglutinin, Nat. Struct. Biol. 8 (2001) 715–721.
[33] R.W. Doms, A. Helenius, J. White, Membrane fusion activity of the influenza virus hemagglutinin, J. Biol. Chem. 260 (1986) 2973–2981.
[34] R.M. Epand, R.F. Epand, Relation between the infectivity of influenza virus and the ability of its fusion peptide to perturb bilayers, Biochem. Biophys. Res. Commun. 202 (1994) 1420–1425.
[35] J. Lüneberg, I. Martin, F. Nüβler, J.M. Ruysschaert, A. Herrmann, Structure and topology of the influenza virus fusion peptide in lipid bilayers, J. Biol. Chem. 270 (1995) 27606–27614.
[36] T.J. McIntosh, A.D. Magid, in: G. Ceve (Ed.), Phospholipids Handbook, Marcel Dekker, New York, 1993.
[37] E.I. Pécheur, J. Sainte-Marie, A. Bienvenüe, D. Hoekstra, Lipid headgroup and peptide penetration, but not peptide oligomerization, modulate peptide-induced fusion, Biochemistry 38 (1999) 364–373.
[38] L.V. Chernomordik, E. Leikina, V. Frolov, P. Bronk, J. Zimmerberg, An early stage of membrane fusion mediated by the low pH conformation of influenza hemagglutinin depends upon membrane lipids, J. Cell Biol. 136 (1997) 81–94.
[39] T. Stegmann, S. Nir, J. Wilschut, Membrane fusion activity of influenza virus: effects of gangliosides and negatively charged phospholipids in target liposomes, Biochemistry 28 (1989) 1698–1704.